

PCCP

Accepted Manuscript



This is an *Accepted Manuscript*, which has been through the Royal Society of Chemistry peer review process and has been accepted for publication.

Accepted Manuscripts are published online shortly after acceptance, before technical editing, formatting and proof reading. Using this free service, authors can make their results available to the community, in citable form, before we publish the edited article. We will replace this *Accepted Manuscript* with the edited and formatted *Advance Article* as soon as it is available.

You can find more information about *Accepted Manuscripts* in the [Information for Authors](#).

Please note that technical editing may introduce minor changes to the text and/or graphics, which may alter content. The journal's standard [Terms & Conditions](#) and the [Ethical guidelines](#) still apply. In no event shall the Royal Society of Chemistry be held responsible for any errors or omissions in this *Accepted Manuscript* or any consequences arising from the use of any information it contains.

Chelerythrine-lysozyme interaction: spectroscopic studies, thermodynamics and molecular modeling exploration

Chandrima Jash^{†¶}, Pritha Basu^{†¶}, Pavan V. Payghan,^{‡¶} Nanda Ghoshal[‡] and Gopinatha Suresh Kumar^{†*}

Biophysical Chemistry Laboratory, Chemistry Division[†] and Structural Biology and Bioinformatics Division[‡]

*CSIR-Indian Institute of Chemical Biology, 4, Raja SC Mullick Road
Kolkata 700 032, INDIA*

Address for Correspondence

Dr. G. Suresh Kumar, Senior Principal Scientist
Biophysical Chemistry Laboratory, Chemistry Division
CSIR-Indian Institute of Chemical Biology
4, Raja S. C. Mullick Road, Jadavpur
Kolkata 700032, INDIA
Phone: +91 33 2472 4049 /2499 5723
Fax: +91 33 2473 0284 / 5197
e-mail: gskumar@iicb.res.in/ gskumar@csiriicb.in

[¶]These authors contributed equally to this work.

[†] Biophysical Chemistry Laboratory, Chemistry Division

[‡]Structural Biology and Bioinformatics Division

Abstract

The binding of the iminium and alkanolamine forms of chelerythrine to lysozyme (Lyz) was investigated by spectroscopy and docking studies. The thermodynamics of the binding was studied by calorimetry. Spectroscopic evidences suggested that Trp-62 and Trp-63, in the β -domain of the protein are closer to the binding site; the binding site was at a distance of 2.27 and 2.00 nm, respectively from the iminium and alkanolamine forms as per Forster theory of non-radiation energy transfer. The equilibrium binding constants for the iminium and alkanolamine forms at 298 K were evaluated to be 1.29×10^5 and $7.79 \times 10^5 \text{ M}^{-1}$, respectively. The binding resulted in alteration of the secondary structure of the protein with a distinct reduction of the helical organization. The binding of the iminium was endothermic involving electrostatic and hydrophobic interactions while that of the alkanolamine form was exothermic and dominated by hydrogen bonding interactions. Docking studies provided the atomistic details pertaining to the binding of both forms of chelerythrine and supported the higher binding in favour of the alkanolamine over the iminium. Furthermore, molecular dynamics study delivered accurate insights about the binding of both the chelerythrine forms in accordance with obtained experimental results. Overall, chelerythrine binding pocket involves catalytic region and aggregation prone K-peptide region which are well sandwiched between one another. Taken together, these results suggest that both forms of the alkaloid bind to the protein but the neutral form has higher affinity than the cationic form.

Keywords: Chelerythrine alkaloid, Lysozyme, Interaction, Spectroscopy, Calorimetry, Molecular modelling

Introduction

Development of natural products as drug candidates has immense advantage due to their high abundance, relatively low toxicity, and excellent biocompatibility. They have an incomparable success rate as lead drug candidates over synthetic compounds. Many of the currently used drugs are essentially from natural sources.¹ Benzophenanthridine alkaloids are a group of molecules with versatile chemistry and diverse biological utility. Chelerythrine (1,2-dimethoxy-12-methyl[1,3]benzodioxolo[5,6-c]phenanthridin-12-ium) (Fig. 1) is an alkaloid of this group isolated from a natural herb called greater celandine *Chelidonium majus L.* It is a potent, selective, and cell permeable protein kinase C (PKC) inhibitor that does not inhibit tyrosine protein kinases, cAMP-dependent protein kinase, or calcium/calmodulin-dependent protein kinases.² The therapeutic potential of chelerythrine in cancer research has also been well documented. It has promising role as antineoplastic growth inhibitor against various tumor cell lines like human breast cancer (MCF-7), human uveal melanoma (OCM-1), human neuroblastoma, colon carcinoma (HCT116) cell lines and neonatal rat cardiac myocytes.³⁻⁷ Recent studies have implicated that PKC-independent mechanism may also be responsible for its potential anticancer property.^{8,9} This might include binding to duplex and quadruplex nucleic acid structures that has been very recently reported.¹⁰⁻¹²

One of the remarkable structural features of the benzophenanthridines is their ability to exhibit pH dependent structural transition between the iminium and alkanolamine forms.¹³ This has been very well demonstrated in the case of sanguinarine,¹⁴ a close analogue of chelerythrine, studied recently for its binding to lysozyme.¹⁵ Although there are only small structural differences between sanguinarine and chelerythrine large functional differences have been observed. For example, sanguinarine is a potent suppressor of NF- κ B activation but chelerythrine has no effect.¹⁶ They bind to different regions of Bcl(XL)¹⁷ and

chelerythrine has been identified as an inhibitor of BclXL-Bak BH3 peptide binding.¹⁸ Therefore, we felt it necessary to examine in depth the binding aspect of chelerythrine with lysozyme.

Lysozyme (N-acetylmuramide glyconohydrolase) is an antimicrobial protein present in abundance in various protective fluids and lymphatic tissues of most animals. It is known for the unique ability to damage bacterial cell wall, by cleaving the β -linkages between the N-acetyl-muramic acid and N-acetyl- glucosamine of the peptidoglycan thereby protecting against bacterial infections. Lysozyme is also widely used as a food preservative and as an antimicrobial agent.¹⁹⁻²¹ Other activities include anti-inflammatory, antiviral, antiseptic, antihistamine and antineoplastic effects. Due to its small size, high stability, natural abundance, propensity to undergo amyloid aggregation and ability to carry drugs, Lyz has been preferred as a model protein in many studies to understand protein folding, structure-function, dynamics and ligand interactions.²²⁻²⁵ The details on the structure of Lyz, domains and amino acids in the protein were described in details in our recent study.¹⁵ The binding of sanguinarine to lysozyme has identified the buckled alkanolamine to bind stronger than the planar iminium.¹⁵ Recently, the binding studies of a number of small molecules, alkaloids, nano particles and model membranes to lysozyme were reported.²⁵⁻²⁸ Such studies are important for developing small molecules that can act as effective inhibitors of aggregation of amyloidogenic proteins.²⁹⁻³⁰

In the present contribution we describe the binding interaction of the two forms of chelerythrine, viz. the iminium and alkanolamine with chicken egg white lysozyme. Initially we used spectroscopy techniques to analyze the binding affinity of the interaction followed by thermodynamic analysis by calorimetric techniques on the energetic aspects. Subsequently molecular modeling and simulation approaches were used to gain deeper insights on the binding site and interactions which govern the binding. This multifaceted approach enabled

us to provide a detailed molecular basis for chelerythrine-Lyz interaction. The results may be helpful to understand the protein binding properties of chelerythrine for use in drug development.

Experimental

Materials

Chicken egg white lysozyme (≥ 98 purity, $M = 14.3$ kDa), chelerythrine (CAS No. 92-31-9, purity $> 95\%$) were from Sigma–Aldrich LLC (St. Louis, MO). The molar absorption coefficient (ϵ) and other optical properties of the alkaloid are listed in Table S1. All other materials and chemicals used in this study were of analytical grade. Deionized water from a Milli-Q water purification system (Millipore, USA) was triple distilled and filtered through $0.22 \mu\text{m}$ Millipore Millex-HV PVDF filters for buffer preparations.

Sample preparation

The protein sample was purified on a CM-cellulose (Sigma-Aldrich) column as reported in the literature.³¹ The sample was then desalted on a Sephadex G-50 column, dialyzed (SpectraPor MWCO, 3500 membrane) and lyophilized. Citrate-phosphate (CP) buffer, pH 6.4, and carbonate-bicarbonate (CB) buffer, pH 9.2, respectively, with 10 mM Na^+ ion concentration were used for the studies with the iminium and alkanolamine forms. The protein sample was dissolved in these buffers for further studies. In these pH conditions the alkaloid solution remained stable as iminium and alkanolamine forms in 100% population. The concentration of the alkaloid in each experiment was kept at the minimum required to prevent aggregate formation and adsorption to the cuvette walls.

The lysozyme concentration was determined using the molar absorption coefficient (ϵ) value of $37,750 \text{ M}^{-1} \text{ cm}^{-1}$ at 280 nm .³² The alkaloid concentration was estimated using ϵ values of $30,700 \text{ M}^{-1} \text{ cm}^{-1}$ for the iminium and $21,600 \text{ M}^{-1} \text{ cm}^{-1}$ for the alkanolamine forms at 327 nm .

Equipments and measurements

pH measurements were made on a Sartorius high precision bench pH meter with a microelectrode (Sartorius GmbH, Germany). The absorption spectra were recorded at 25 ± 1.0 °C on Jasco V660 unit (Jasco International Co., Hachioji, Japan) using matched 1.0 cm quartz cuvettes.

Steady-State fluorescence measurements

Steady state fluorescence spectra were measured on either a Shimadzu RF-5301 PC (Shimadzu Corporation, Kyoto, Japan) or a Hitachi F4010 (Hitachi Ltd., Tokyo, Japan) fluorescence spectrophotometer in fluorescence free quartz cuvettes of 1 cm path length. The excitation and emission slit widths for all measurements were set up at 5 and 10 nm, respectively. The sample temperature was maintained at 25 ± 1.0 °C using Eyela UniCool U55 water bath (Tokyo Rikakikai Co. Ltd., Tokyo, Japan).

Intrinsic fluorescence was measured by exciting Lyz at 295 nm because tryptophan fluorescence is generally used as a probe of local environment changes of protein structure, dynamics as well as ligand binding as this exclusively excites the intrinsic tryptophans (Trp). Chelerythrine iminium and alkanolamine forms were excited at 338 and 318 nm, respectively. Temperature dependent fluorescence spectral studies were performed on the Hitachi F4010 unit. Synchronous fluorescence was measured in the excitation range of 220–380 nm keeping $\Delta\lambda$ set at 15 and 60 nm, respectively.

Time resolved fluorescence lifetime measurements

The lifetime measurements were performed using time-correlated single photon counting (TCSPC) technique in a Horiba Jobin Yvon FluoroCube fluorescence lifetime systemt at 25 ± 1.0 °C. The excitation was done at 295 nm using a pico second diode laser (IBH N-295) in an IBH fluorocube apparatus. The emission data were collected at a magic angle (54.7°)

relative to the excitation. The instrumental response function was determined experimentally on the basis of light signal scattered from Ludox (colloidal silica in water) and was used for subsequent deconvolution of the fluorescence signal. The decays were deconvoluted using IBH DAS6 decay analysis. The fits were judged by χ^2 criteria and visual inspection of the residuals of the fitted function to the data. The fluorescence decay was described as a sum of exponential functions as follows³³

$$F(t) = \sum a_i \exp(-t/\tau_i) \quad (1)$$

Here, $F(t)$ is the fluorescence intensity at time t and a_i is the pre-exponential factor corresponding to the i th decay time constant, τ_i . For multi exponential decays, the average lifetime τ_{avg} was calculated from the following relation³³

$$\tau_{\text{avg}} = \sum a_i \tau_i \quad (2)$$

Here, τ_i is the fluorescence lifetime and a_i the relative amplitude with i variable from 1 to 2.

Hydrophobic probe displacement study

For extrinsic ANS displacement study, in the first series of experiments, the Lyz concentration was kept fixed at 1.0 μM , the chelerythrine/ANS concentration was varied from 1.0 to 10 μM , and Lyz fluorescence was monitored ($\lambda_{\text{ex}} = 295 \text{ nm}$, $\lambda_{\text{em}} = 339 \text{ nm}$). In the second series of experiments, chelerythrine was added to solutions of Lyz and ANS held in equimolar concentration (1.0 μM each); the concentration of chelerythrine was also varied from 1.0 μM to 10 μM and the fluorescence of Lyz was recorded ($\lambda_{\text{ex}} = 295 \text{ nm}$, $\lambda_{\text{em}} = 339 \text{ nm}$).

Circular dichroism spectroscopy

Secondary and tertiary structural changes (CD spectra) in the protein on interaction with chelerythrine were measured on a Jasco J815 spectropolarimeter (Jasco International Co, Hachoji, Japan). A Peltier cell holder and temperature controller PFD 425 L/15 maintained the cuvette temperature at 25°C. The CD spectra were acquired with sensitivity set to 10 milli

deg and a scan speed of 50 nm/min with step size of 0.5 nm. The time constant was 1 sec and bandwidth was 0.2 nm. Five successive scans were performed to improve the signal-to-noise ratio, smoothed within permissible limits and base line corrected. The molar ellipticity values were expressed in terms of the mean residue molar ellipticity (MRE), in units of deg cm² dmole⁻¹.

Isothermal titration calorimetry

A VP ITC unit (MicroCal, Inc., Northampton, MA, USA) was used for calorimetric experiments. Lyz and alkaloid solutions were degassed on the Thermovac unit. The rotating syringe of the unit was filled with a solution of the Lyz (0.8 mM for iminium and 0.5 mM for alkanolamine). Programmed injections of 10 μL aliquots of Lyz solution were effected into the iminium and alkanolamine solutions of alkaloid in the calorimeter cell. The data were corrected for the heats of dilution of the protein and the alkaloid, which were determined in separate set of experiments under identical buffer conditions and temperature.

The “one set of sites” model yielded the best fit curve for the obtained experimental data points in all the cases. Equilibrium association constant (K_b), enthalpy change (ΔH°) and entropy contribution ($T\Delta S^\circ$) of the interactions were determined by fitting the isotherms to the model. Standard molar Gibbs energy (ΔG°) was calculated using the equation

$$\Delta G^\circ = \Delta H^\circ - T\Delta S^\circ \quad (3)$$

where T is the absolute temperature in Kelvin and R is the gas constant (1.9872041 cal. mole⁻¹. K⁻¹).

Molecular modeling study

Binding mode analysis of iminium and alkanolamine forms of the alkaloid was undertaken using Induced Fit Docking (IFD) technique from Schrodinger Maestro-v96012 9.6 suite.³⁴ Crystal structure of Lyz was obtained from RCSB Protein Data Bank (PDB 2LYZ, with resolution of 2.0 Å).³⁵ We performed in vacuo docking by removing all the water molecules

from the crystal structure. The ligand structures for alkanolamine and iminium forms were built with Maestro. To obtain stable structures from built structures we performed simulated annealing and energy minimization. Ligand and protein were subjected for preparation using LigPrep and Protein Preparation Wizard. During protein preparation, hydrogens were added considering the correct bond orders. Two different protein states were generated considering pH condition of 6.4 and 9.2, respectively. Obtained structures were subjected for restrained minimization with OPLS-2005 force field and convergence criterion of 0.30 Å.

During ligand preparation, ionization states were assigned using ionizer module to set pH condition of 6.4 and 9.2, respectively, for iminium and alkanolamine forms. Previously known sanguinarine binding site was defined for these close analogs guided by previous experimental reports.^{15,36-39} Box of 24 Å was defined for Glide grid setup. Box centre was defined with the centroid of residues, Arg-45, Asn-46, Arg-61, Trp-62, Trp-63, Trp-108, Val-109 and Ala-110, which form this binding site. Glide soft potential docking was carried out using van der Waals radii scaling of 0.7 for receptor and 0.5 for ligands respectively. Side chains of the residues were trimmed based on automatic B-factor values to maximize the interaction probability. This step generated 20 ligand poses with SP (Single Precision) mode. Prime induced fit refinement was employed for the residues within 24 Å of the ligand poses using OPLS parameters. Glide XP (Extra Precision) redocking was performed for 20 obtained protein conformations with default hard potential function and van der Waals radii scaling of 1.0. Final selection of best pose was performed on top ranked poses keeping in mind the presence of important interactions. In order to check the reproducibility of obtained results we repeated same IFD experiment for four times for each form, giving in total 5 runs for each of the forms. In all the cases we found presence of our selected pose. Further we took binding free energy scores (GlideScore) for all the generated poses in five IFD runs for

each of the cases and performed cluster analysis to find Lyz-ligand complexes with minimum Glide Score.

Result visualization was done with Pymol,³⁹ Discovery Studio 4.0⁴⁰ and Swiss PDB viewer.⁴¹

Molecular dynamics simulation studies

We performed molecular dynamics (MD) studies on the above selected poses for the dynamic considerations. We carried out all atom molecular dynamic simulations using Gromacs 4.6.7⁴² with GROMOS 53a6⁴³ force field. Three systems were prepared consisting each of the Lyz-apo, Lyz-iminium and Lyz-alkanolamine forms. Topology and charge information for the ligands was obtained from Automated Topology Builder version 2.1^{44,45}. Systems were solvated using SPC⁴⁶ water model in a cubic box of size $\sim 72.3 \times 72.3 \times 72.3$. Then it was neutralized to final physiological concentration of 100 mM by adding Na^+ and Cl^- counter-ions. Energy minimization of 5000 steps was employed with steepest descent method. Both NVT followed by NPT equilibration was performed for 100ps using position restrained protein and protein-ligand complexes, for apo and bound complexes respectively. During NVT, v-rescale⁴⁷ temperature coupling was employed at 300 K. NPT was performed with parrinello-rahman⁴⁸ pressure coupling with isotropic scaling at 1 bar pressure. Electrostatic treatment for long range interactions was taken care by Particle Mesh Ewald sum method.⁴⁹ For constraining all the heavy atoms including heavy atom hydrogen LINCS⁵⁰ algorithm was employed. Neighbor searching was performed using verlet cut-off scheme⁵¹ having short range electrostatic cut-off of 1.2 nm. In unrestrained systems production runs were performed using NPT ensemble and with time step of 2 fs. In total 300ns data was generated for all three systems. Initial 10ns data was taken as equilibration period and remaining 90ns data was considered for performing the analysis.

Results and discussion

UV-vis absorption spectroscopy study

Detailed absorption spectral characterization of chelerythrine was described in our earlier studies with nucleic acids.⁵² Briefly, the visible absorption profile of the iminium and alkanolamine forms are characterized by distinguishable absorption spectral patterns (Fig. 1). The iminium form (pH 6.4) has peaks at 273, 328 and 469 nms while the alkanolamine (pH 9.2) has peaks at 234, 283 and 326 nms. The protein, on the other hand, at both pH conditions is characterized by two absorption maxima, one strong peak around 200 nm and a weak peak around 281 nm.²⁷ Absorption spectral changes were used to explore the binding of the alkaloid to the protein and the same are presented in Fig. 2A,B. The characteristic absorption peak around 200 nm arises due to the peptide bonds of the protein while the 281 nm peak is due to the aromatic amino acids (Trp and Tyr). In the presence of increasing concentration of chelerythrine, there was a decrease of the intensity of the peaks, with a red shift of the 281 nm peak for both the forms. Similar type of results were reported¹⁵ for Lyz on binding of sanguinarine and other small molecules.^{15,27} This change indicates that the binding of the alkaloid forms induced an unfolding of the protein backbone. It is likely that an increase in the hydrophobicity of the microenvironment of the aromatic amino acids occurs on chelerythrine interaction.

The absorbance data were analyzed by the Benesi-Hildebrand equation,⁵³

$$1/\Delta A = (1/\Delta A_{\max}) + \{(1/K_{BH}\Delta A_{\max}) (1/[M])\} \quad (4)$$

where K_{BH} is the binding constant and $[M]$ is concentration of the quencher (chelerythrine). Fitting to this equation gave linear plots (inset of Fig. 2A and 2B) in both the cases with K_{BH} values of 1.19×10^5 and $5.85 \times 10^5 \text{ M}^{-1}$, respectively, for the iminium and alkanolamine forms. This result clearly suggests that the affinity for Lyz is higher for the alkanolamine form compared to the iminium form.

Fluorescence spectral studies: alkaloid induced fluorescence quenching of lysozyme

Fluorescence emission profile of the fluorophore of the protein can provide detailed information on the binding of small molecules in terms of the nature and mode of the interaction.^{54,55} A detailed description of the Trp residues present in Lyz and their locations were described in our earlier report on sanguinarine binding.¹⁵ The excitation of the protein was performed at 295 nm exciting the Trp moieties, particularly Trp-62 and 63, giving emission spectrum with maximum around 340 nm. Figure 3A, B portrays the fluorescence spectral changes of Lyz in the presence of iminium and alkanolamine forms. Increasing concentration of the alkaloid leads to quenching of the fluorescence of Lyz, the effects reaching saturation eventually in both cases. A bathochromic shift of the fluorescence peak was observed that may be assigned to the exposure of the Trp side-chain(s) to a more hydrophilic environment due to the slight unfolding of lysozyme from binding of the alkaloid.^{56,57} A correction for the inner-filter effect of chelerythrine on Lyz was performed before analysis of the data. The inner filter effect was corrected as described by MacDonald et al.⁵⁸ using the equations described in details recently.⁵⁹

To distinguish between the collisional quenching (dynamic) and binding-related quenching (static)⁵⁹ temperature dependent studies were performed at three temperatures viz., 288, 298 and 308K. It is known that at higher temperatures larger diffusion coefficients occur and the dynamic quenching constants will increase. On the other hand, in the case of static quenching temperature increase may lead to decreased stability.

The data were analyzed by the classical Stern-Volmer equation⁵⁹

$$\frac{F_0}{F} = 1 + k_q \tau_0 [Q] = 1 + K_{SV} [Q] \quad (5)$$

where F_0 and F are the fluorescence intensities at the wavelength maxima in the absence and in the presence of chelerythrine, k_q is the bimolecular quenching constant, K_{SV} is the Stern-Volmer quenching constant, τ_0 is the average life time of the protein in the absence of

quencher which is taken to be 2.08 ns at pH 6.4 and 1.95 ns at pH 9.2 and $[Q]$ is the concentration of the quencher, respectively.⁶⁰ Figure S1 shows the linear Stern-Volmer plots of F_0/F versus $[Q]$ at the three temperatures and the calculated K_{sv} and k_q values are summarized in Table 1. The results revealed that the values of K_{sv} and k_q decreased with increasing temperature, and the k_q values are $> 2.0 \times 10^{10} \text{ M}^{-1} \text{ s}^{-1}$. This data suggests that quenching mechanism is clearly due to static quenching for both iminium and alkanolamine forms of chelerythrine.⁶⁰ In other words, the protein fluorescence quenching in the presence of chelerythrine is due to specific complex formation at the ground state. Similar result was observed for the binding of sanguinarine also.¹⁵

Chelerythrine iminium and alkanolamine forms exhibit emission spectra with maxima at 551 nm and 419 nm, respectively, when excited at 338 and 316 nms (Fig. 4A). We studied the effect of Lyz on the fluorescence of chelerythrine (Fig. 4B). Quenching of the fluorescence intensity was higher in the case of alkanolamine form compared to iminium form suggesting stronger interaction of the former with Lyz. This result also suggested better binding of the alkanolamine form compared to the iminium and is similar to that observed for sanguinarine.¹⁵

Binding constants and number of binding sites of chelerythrine-Lyz complex

The above fluorescence quenching results indicated specific interaction between the alkaloid and the protein leading to strong complex formation. So assuming binding of the alkaloid independently to a set of equivalent sites on the protein the equilibrium binding constant (K_A) and the number of binding sites (n) can be determined from the following equation²⁷

$$\log \frac{(F_0 - F)}{F} = \log K_A + n \log [Q] \quad (6)$$

where K_A is the binding constant to a site and n is the number of binding sites on the protein. From the linear plots of $\log (F_0 - F)/F$ versus $\log [Q]$ (figure not shown) for iminium and

alkanolamine, binding affinity values to Lyz at the three temperatures are presented in Table 1. A higher binding affinity of the alkanolamine ($7.26 \times 10^5 \text{ M}^{-1}$) compared to the iminium ($1.21 \times 10^5 \text{ M}^{-1}$) was apparent from this data. The magnitude of the values of K_A suggests the occurrence of a moderate interaction between chelerythrine with Lyz and the alkanolamine form has a higher affinity to the protein. The numbers of binding sites obtained from the magnitudes of 'n' values were found to be around unity suggesting that there is only one kind of binding site for these two forms, most likely around the Trp residue of the protein. The 1:1 binding of these alkaloids on Lyz was further confirmed from Job's plot analysis by fluorescence spectroscopy data by varying the alkaloid: protein molar ratio while keeping the total molar concentration constant. The difference in fluorescence at 339 nm *versus* mole fraction of alkaloids (χ) (Fig. S2) crossed at 0.49 and 0.485, respectively, for the iminium and alkanolamine forms of chelerythrine yielding the number of each of these molecules binding on the protein to be around 1.

The quenching data was also analyzed by the Lineweaver-Burk equation²⁷

$$\frac{1}{(F_0 - F)} = \frac{1}{F_0} + \frac{1}{K_{LB}F_0[Q]} \quad (7)$$

where the quenching constants (K_{LB}) were obtained from the ratio of the intercept to slope of the Lineweaver-Burk plot, describing the efficiency of quenching at the ground state. The plots of Lyz-chelerythrine interactions at three temperatures are presented in Fig. S3 (Supporting Information). The data depicted in Table 1 revealed that alkanolamine form has the higher affinity to Lyz than the iminium. Furthermore, the variation of K_{LB} with increasing temperature was similar to those of K_{SV} values and is consistent with the static quenching mechanism.

Energy transfer from Lyz to the bound chelerythrine

It is well-established that a strong ligand-protein complexation may lead to transfer of excited energy from the donor (protein) to the acceptor (ligand). Apart from divulging on the binding aspects measurement of energy transfer efficiency can provide an idea about the distance of separation between the bound ligand and the site of interaction on the protein.²⁷ The proximity of the ligand molecule to the Trp moiety of the protein can be determined through fluorescence resonance energy transfer (FRET) study. By Förster theory the efficiency depends on the extent of overlap of the donor emission and acceptor absorption, orientation of the transition dipole of the donor and the distance between the donor and acceptor which must be within 2-8 nm.²⁷ The efficiency (E) of the FRET process depends on the inverse sixth power of the distance between donor and acceptor (r) and of the critical energy transfer distance or Förster radius (R₀). When the efficiency of transfer is 50%, a condition of 1:1 situation of donor to acceptor concentration prevails and E, the energy transfer efficiency, is expressed by the equation

$$E = 1 - \frac{F}{F_0} = \frac{R_0^6}{R_0^6 + r^6} \quad (8)$$

R₀ can be calculated using the relation

$$R_0^6 = 8.8 \times 10^{-25} \kappa^2 n^{-4} \phi J \quad (9)$$

$$\text{Where, } J = \frac{\int_0^{\infty} F(\lambda) \varepsilon(\lambda) \lambda^4 d\lambda}{\int_0^{\infty} F(\lambda) d\lambda}$$

here κ^2 is the space factor of orientation, n is the refractive index of the medium, ϕ is the fluorescence quantum yield of the donor. F(λ) represent the fluorescence intensity of the donor and $\varepsilon(\lambda)$ the molar absorption coefficient of the acceptor, respectively, at the wavelength λ . Using the values of $\kappa^2=2/3$, n = 1.336 and $\phi = 0.14$ for Lyz,²⁷ the values of E, J,

R_0 and r have been calculated to be 0.49, $2.36 \times 10^{-14} \text{ cm}^3 \cdot \text{L} \cdot \text{mol}^{-1}$, 2.69 nm and 2.70 nm for iminium-Lyz and 0.73, $8.54 \times 10^{-15} \text{ cm}^3 \cdot \text{L} \cdot \text{mol}^{-1}$, 2.27 nm and 2.0 nm for alkanolamine-Lyz interaction from the overlap of the absorbance spectra of the alkaloid with the emission spectrum of Lyz (Fig. S4). The distance between the ligands and the amino acid residue Trp in Lyz is far lower than 8 nm, the upper limit indicating high probability of energy transfer from the Trp residues of the protein to the alkaloids.²⁷ Moreover, it demonstrates that all the conditions of energy transfer theory are obeyed; (i) Lyz can produce fluorescence light (Fig. 3), (ii) sufficient overlap is observed between the fluorescence spectrum of Lyz and the UV-vis spectra of chelerythrine forms (Fig. S2), and (iii) the value of the distance in both systems is less than 8 nm. The results highly support that the binding of chelerythrine to Lyz is through energy transfer, leading to formation of ground-state complexes. Hence, further analysis to determine the parameters such as the binding constant and number of binding sites of chelerythrine-Lyz complexation is feasible.

Fluorescence lifetime study

Time resolved fluorescence decay of Lyz was recorded in the presence of chelerythrine to understand the effect of the alkaloid on the protein dynamics. From the time-resolved fluorescence decay profiles of Lyz in the absence and presence of chelerythrine (not shown) the fluorescence lifetime values and their amplitudes were calculated. The decay curves fitted well to a bi-exponential function with an emerging average fluorescence lifetime values of $\tau = 2.08 \text{ ns}$ and $\tau = 1.95 \text{ ns}$, respectively, for Lyz at pH 6.4 and 9.2. After the addition of maximum concentration of chelerythrine iminium and alkanolamine forms (100 μM) to Lyz, the observed average fluorescence lifetime values were $\tau = 1.81 \text{ ns}$ and 2.07 ns, respectively. Trp residue is known to divulge multi exponential decays, but a clear allocation of the perceived separate fluorescence lifetime components to the disparate fluorescent Trp residues is hard to determine for lysozyme with multiple Trp residues.⁶¹ Consequently we have not

tried to designate the individual components; conversely, the average fluorescence lifetime has been exploited to gain a qualitative analysis. The average fluorescence lifetime of Lyz did not alter significantly at the maximum concentration of chelerythrine. The static quenching mechanism is generally associated with stable fluorescence life time values while in dynamic quenching the fluorescence life time values alter significantly.³³ The time resolved fluorescence results clearly indicated that the fluorescence lifetime of Lyz complexed with both iminium and alkanolamine forms of chelerythrine was almost unperturbed. This result confirms that the quenching of Lys-chelerythrine emission is primarily static in nature and due to complex formation at for both iminium and alkanolamine forms.⁶¹⁻⁶³

Steady-state fluorescence anisotropy study

Steady state anisotropy data may provide valuable information on the degree of motional restriction of the fluorophore and is used as a probe to assess the extent of flexibility or tumbling of small molecules after binding. The basis of fluorescence anisotropy to interpret on the environment in the immediate vicinity of the fluorophore is based on the fact that larger molecules tumble more slowly while smaller molecules tumble faster. An increase in fluorescence polarization anisotropy of chelerythrine on binding to Lyz is as a result of increased motional restriction of chelerythrine consequent to strong binding. On binding, the anisotropy value of the alkanolamine form increased from 0.01 to 0.04. The anisotropy change in the case of iminium was only marginal suggesting that the motional rigidity imposed here is much less than that of the alkanolamine form. This data provided information on the stronger interaction of the alkanolamine to the protein compared to the iminium.

Hydrophobic probe ANS displacement study

The fluorescent dye 8-anilino-1-naphthalenesulfonic acid (ANS) is a hydrophobic probe sensitive to microenvironment changes and has often been used to extract information on the hydrophobic binding regions on the protein surfaces.⁶⁴ The goal of executing the ANS studies

was to further confirm the region of chelerythrine binding on the protein Lyz. According to the protocol, binding studies were executed in the presence of ANS under identical conditions, and the relative fluorescence (F/F_0) against ligand concentration was plotted, as shown in Fig. 5. Evidently, at a ligand concentration of 10 μM , chelerythrine had a better quenching effect on fluorescence of the protein than ANS, i.e. chelerythrine could quench about ~96%, and ANS approximately 28%. When chelerythrine was added to the ANS–Lyz complex, the fluorescence of ANS–Lyz decreased by nearly 75 %. Stryer^{64,65} has described that interaction of ANS with solvent exposed hydrophobic clusters of a protein would result in a considerable augmentation of fluorescence of ANS. Here, the fluorescence intensity of ANS–lysozyme complex was reduced by 75% by chelerythrine, indicating that chelerythrine can compete with ANS very moderately for its binding site leading to a decrease of the ANS–Lyz fluorescence.

Conformational studies: synchronous fluorescence spectroscopy

Conformational changes during ligand binding to protein can be determined using synchronous fluorescence.⁶⁶ According to the theory of Miller,⁶⁷ when the difference values between the excitation and emission wavelengths ($\Delta\lambda$) are stabilized at 15 or 60 nm, the synchronous fluorescence spectra of the protein provides characteristic information about Tyr and Trp residues. The quenching of protein fluorescence caused by the ligand then implies alteration of the polarity around these amino acid residues. The effect of chelerythrine on the synchronous fluorescence of Lyz with $\Delta\lambda = 60$ nm revealed that the fluorescence intensity diminished systematically with a large red shift of the emission maximum by 8 nm for iminium and 7 nm for alkanolamine binding to Lyz (Fig. S5). A large red shift is indicative of the change of Trp residues to a more hydrophilic environment and more exposed to solvent in both the cases. Comparatively, there is almost no shift in the maximum emission wavelength using $\Delta\lambda = 15$ nm for both iminium and alkanolamine forms showing that little

transformation takes place in the microenvironment around tyrosines. This indicates that in the presence of both the forms of chelerythrine, Trp residues are more exposed to solvent compared to the tyrosines. Therefore, the binding of the chelerythrine changed the polarity around the Trp residues, and most likely that around Trp-62 and Trp-63, while that around Tyr residues was unaffected in agreement with the results from fluorescence quenching and FRET experiments. This result implicates, unequivocally, the involvement of Trp residue in the binding process.

Conformational studies: circular dichroism spectroscopy

Evidence for conformational changes in Lyz upon interaction of chelerythrine was obtained from the change in the CD spectra. Chicken egg white lysozyme is an $\alpha + \beta$ protein with a large α -domain containing four α -helices and a 3_{10} -helix and a smaller β -domain consisting of a triple-stranded anti-parallel β -sheet, an irregular loop containing two disulphide bridges and a 3_{10} -helix. The deep active cleft of the protein divides the enzyme into two domains, one of them is mostly β sheet structure and the other contains N and C-terminal segments that is mostly alpha helical. The far ultraviolet CD spectrum of native Lyz contained two minima at 208 nm and 222 nm, characteristic of a predominantly α -helical structure and is in agreement with previous observations.²⁷ The 208 nm band corresponds to π - π^* transition of the α -helix and the 222 nm band due to n - π^* transition for both the α -helix and random coil. Upon titration with increasing concentrations of alkaloids, the far-UV CD spectrum of Lyz decreased in intensity without any shifts in the peaks, indicating a decrease in the helical structure (Fig. 6 A, B) suggesting that the binding of the two form of the alkaloid induced secondary structural changes in the conformation of Lyz. Both alkaloid forms are optically inactive and hence do not possess any CD spectra in the region of the study. The helical

content of the free and bound Lyz molecules were calculated in terms of mean residue ellipticity (MRE) ($\text{deg.cm}^2.\text{dmole}^{-1}$) as reported.²⁷

The alpha helical content of the free and alkaloid bound Lyz was calculated from the ellipticity value at 222 nm. The helical content of Lyz was calculated according to the equation given in the literature²⁷ and it was found to be 35.99% and 36.15%, respectively, in pH 6.4 and 9.2 buffers and close to that reported in earlier observations.

At saturation, corresponding to 30 μM , for both cases, the α -helical content was reduced to 25% and 22%, respectively. Thus, the unfolding and loss of the helical stability has been observed on binding inducing strong secondary structural changes in the protein. It appears that interaction with the chelerythrine leads to an unfolded conformation of Lyz exposing the hydrophobic cavities with concomitant exposure of the aromatic amino acid residues and the observed change is more in case of the alkanolamine form.

In order to understand any changes in the tertiary structure of Lyz induced by the binding of these forms of the alkaloid, we carried our near-UV CD spectral experiments. The CD spectra in the in the near-UV region (250-300 nm) arises due to the presence of disulphide bonds and the aromatic chromophores (Trp, Tyr, Phe).²⁷ The CD signals at 283, 289 and 295 nm of Lyz are assignable to transitions of the Trp residues.²⁷ In the presence of the alkaloids there were very small changes in the spectral pattern (Fig. S6 A,B) in this region indicating that changes in the environment of the aromatic amino acid side chains due to binding with the indole rings of the tryptophan residues, 62, 63 or 108, the former two lying on the molecular surface and the latter at the end of the cleft leading to a small unfolding of the tertiary structure of the protein and/or enhanced flexibility. It appears that the alkaloid binding does not induce major tertiary structural changes, which is understandable as no break in the disulphide bonds occur. Although the interpretation of the changes is not conclusive, in conjunction with the far UV spectral changes and other spectroscopic results it gives some indication on the strong

interaction of the alkaloids with the protein. It is worth mentioning here that the alkaloids did not acquire any induced optical activity on binding to Lyz molecules.

Thermodynamics of the binding from isothermal titration calorimetry

Comparative analysis of the binding of chelerythrine with Lyz will help us to visualize the energetic scenario. Representative thermograms for titration of the iminium and alkanolamine forms to Lyz at 25 °C are shown in Fig. 7 A, B and the corresponding dilution profile in proper scale are depicted in Fig. S7 (A, B). The results obtained from these thermograms are summarized in Table 2. The observations from the figure and the data presented in Table 2 could be summed up as follows. The binding is an endothermic process for the iminium form while it is exothermic for the alkanolamine form. The endothermic reaction may arise essentially from hydrophobic interactions while the exothermic one may be arising from electrostatic interactions; the former is weaker than the later.⁶⁸ It is likely that the charged protein interacts with the cationic ligand through predominantly hydrophobic interactions. A positive value of ΔH° demonstrates the existence of hydrophobic interactions. On the other hand, the neutral protein and neutral ligand (alkanolamine) interaction may take place predominantly via hydrogen bonding interactions and the exothermic nature of the reaction suggests this. Similar parameters were reported from our laboratory for the association of sanguinarine with Lyz. The binding constant of iminium at 298 K was evaluated to be $(1.29 \pm 0.08) \times 10^5 \text{ M}^{-1}$ while the same for the alkanolamine form was $(7.79 \pm 0.08) \times 10^5 \text{ M}^{-1}$. This trend is consistent with the earlier report for sanguinarine, but the magnitudes are higher, particularly in the case of alkanolamine the affinity is twice higher than sanguinarine. The higher binding of the alkanolamine over the iminium to Lyz was evident from the calorimetric data was also obtained from fluorescence studies and the binding affinity values from both techniques are in excellent agreement. Both iminium and alkanolamine forms bind to Lyz in a 1:1 ratio as revealed from the N values. It may be recalled that the binding

stoichiometry for chelerythrine was around 1.0 from Job plot data (Fig. S2). In both the cases reaction was entropy driven, but with a small favorable entropy change in case of alkanolamine form. The favorable negative enthalpy contributions make the association tighter in this case. On the other hand, the iminium binding was entropy driven with a small unfavorable enthalpy contribution. The forces driving the interaction between the alkaloid and the protein were examined as a function of temperature (288-308 K). Overall, with increase in the temperature, the affinity values decreased. The negative enthalpy of binding at all the temperatures indicated favorable exothermic binding of the alkanolamine form with Lyz. With increase of the temperature, the entropy contributions decreased but enthalpy value becomes more negative, so ΔG° remained more or less invariant. This suggests that the binding is driven by dominant enthalpy contributions for alkanolamine form. In the case of iminium, the entropy contributions decreased with increasing temperature but remained a favorable factor to the binding as positive enthalpy of binding decreased with temperature i.e., the reaction is endothermic at higher temperatures due to the structural reorganization of the protein.

The heat capacity changes (ΔC_p°) accompanying the binding can valuable insights into the type and magnitude of binding forces involved in the interaction. The heat capacity change was obtained by the first derivative of temperature dependence of enthalpy change and the data were plotted as ΔH° versus temperature (Fig. S8). The ΔC_p° values for the binding of iminium and alkanolamine to Lyz are -5.72 and -30.3 cal/mole·K, respectively. The values indicate that the binding is specific and accompanied by the burial of non polar surface area.⁶⁹ The observed enthalpy values varied linearly in the experimental range 288–308K studied (Fig. S8), indicating that there is no measurable shift of the pre-existing equilibrium between the conformational states of the protein in the temperature span studied. A high ΔC_p° value is usually associated with changes in hydrophobic or polar group hydration due to dominant

hydrophobic effect in the binding process. Here the magnitude of ΔC_p^0 value for Lyz-iminium interaction is relatively small and negative, whereas that for Lyz-alkanolamine interaction is higher in magnitude. This indicates the involvement of a hydrophobic desolvation effect in the protein upon ligand binding; hydrophobic interactions between the ligand and the active site may also play a major role for alkanolamine binding. Enthalpy-entropy compensation was observed in both the cases in the temperature range studied.

Binding modes from docking studies

Information about putative binding pocket for benzophenanthridine alkaloids have been reported earlier.¹⁵ This orthosteric site is situated near the catalytic region involving residues Glu-35, Asn-44, Asn-46, Thr-47, Asp-52, Gln-57, Trp-62, Trp-63, Ala-107, Trp-108 and Val-109. Docking experiments were performed on Lyz and benzophenanthridine derivatives iminium and alkanolamine form at pH value of 6.4 and 9.2, respectively. Alkanolamine form exists in two enantiomeric states due to the carbon which holds -OH group. We performed IFD on both R and S enantiomers to check their binding preferences.

Lysozyme protein contains six Trp residues out of which three have role in the formation of chelerythrine binding pocket. Residue Trp-63 marks the starting of substrate-binding hinge region and exhibit lesser solvent accessibility compared to the fully exposed Trp-62 (Fig. 8A, B). Trp-108 is buried and forms core of hydrophobic pocket. Hydrophobic pocket is further contributed by residues Ala-107 and Val-109 which are situated at helix-loop junction. Apart from Trp-62/63 the solvent exposed side of binding pocket involves residue Glu-35, Asp-52, Asn-44, Gln-57. Asp-52 is the counterpart of Glu-35, the catalytic diode of Lyz active site. The catalytic diode performs catalytic hydrolysis of β -1,4 glycosidic bond of peptidoglycans from gram positive bacterial cell wall.⁷⁰

Molecular recognition event involves H-bonding (classical and non-classical), electrostatic interaction and hydrophobic interaction. Results are presented in the same order to explain the contribution of each of them for binding of benzophenanthridine alkaloids (Fig. 9 A, B).

Based on our modeling study we found more H-bond interactions for alkanolamine over the iminium form. Trp-63 mediated H-bond was present for both the alkanolamine and iminium forms (distance of 1.88 and 1.93, respectively) indicating need for Trp-63 as a crucial binding partner. For alkanolamine form two more (altogether 3) H-bonds were present at Glu-35 and Arg-114. Hydroxyl group mediated H-bond at the catalytic diode with Glu-35 seems to be required for higher activity as it was only present for alkanolamine which is in accordance with our activity data (1.29×10^5 and $7.79 \times 10^5 \text{ M}^{-1}$, respectively, for the iminium and the the alkanolamine forms. Other non-classical carbon mediated (C-mediated) H-bonds were also found. They are a kind of weaker H-bonds compared to the classical ones and they are known to have a role in binding.⁷¹ We witnessed such large number of H-bonds for alkanolamine over iminium form. In the case of alkanolamine, those were present for both the important residues Asp-52 and Trp-108 along with hydrophobic Ala-107 residue. However, for the iminium, it was present only for Gln-57.

Hydrophobic and electrostatic interactions for both the forms are shown in Figure 8. Hydrophobic surface comparison at the binding site suggests two methoxy groups of alkanolamine form are placed deeply inside the hydrophobic pocket showing maximum occupancy. However, for alkanolamine one of the methoxy groups is placed outside the hydrophobic pocket with shallow positioning and reduced occupancy. Chelerythrine iminium holds hydrophobic interactions with Trp-62, Ala-107 and Val-109 while for alkanolamine it exists at central Val-109 and Asn-46 residue.

Solvent exposed side permits electrostatic interaction at Asp-52 and is present for both forms of the alkaloid. It is a key interaction that affects catalysis of Lyz protein. Asp-52 mediated

interactions are present across majority of the alkanolamine ring system which place it correctly thereby allowing Glu-35 H-bond on one side and well distributed electrostatic interactions on another side. Interactions at catalytic diode, Glu-35 and Asp-52, can directly affect the catalytic function of Lyz; our data support its prominent presence for alkanolamine over the iminium form.

Our analysis indicates that for proper binding, dimethoxy side of benzophenanthridine alkaloid has to orient towards the hydrophobic pocket while the opposite side remains facing the solvent exposed area. Functional group in the middle of the ring system must remain facing the binding pocket in order to facilitate maximized interactions.

The binding interactions along with the docking scores have been shown in Table 3. Based on our in vacuo modeling and IFD docking we found maximum interactions for alkanolamine- at the orthosteric site than for the iminium form. GlideScore based cluster analysis of Lyz- ligand complex structures revealed the presence of selected poses in one cluster of minimum GlideScore out of 3 clusters in each case.

We explored results of static docked poses to obtain their dynamic level information using molecular dynamics (MD) simulation.

Dynamic view from MD studies

The static docked complexes were further evaluated for stability and structural changes using MD simulations to sample the relevant conformational space. The first measure of stability is root mean square deviation (RMSD) calculations considering the backbone atoms (shown in Fig. 10).

For most of the simulation time RMSD ranges near ~ 0.35 nm for all three systems. When we focus on first 40ns run, Lyz-iminium form complex carries marginally less RMSD than the apo state showing stability imparted due to iminium form binding. However, for Lyz- alkanolamine form complex RMSD tend to rise up sharply reaching the max value of 0.4 nm

for a fraction of time followed by stable value at 0.35 nm. Up to this point alkanolamine form binding triggers the maximum possible Lyz structural changes, reflected as high RMSD value. As we move further, overall stable and overlapping RMSD for all three systems is apparent. RMS deviation between starting and end structure at 100ns (for backbone atoms) was found to be 1.60, 1.62, and 1.73 for Lyz-apo, Lyz-iminium form and Lyz-alkanolamine form complexes, respectively. It indicates higher structural perturbation after alkanolamine form binding.

To report the compactness of Lyz structure we calculated radius of gyration (R_g) for ligand unbound and bound states (Fig. 11). R_g values for all the three systems lie within 1.38 - 1.46 nm. This indicates along the entire trajectory Lyz structure for both unbound and bound states remain largely the same without any significant conformational change.

To locate the region of structural fluctuations, Root Mean Square Fluctuation (RMSF) calculations were carried out (shown in Fig.12). RMSF for Lyz-apo state provides baseline for comparing the fluctuations with iminium or alkanolamine form bound complexes. Analysis result indicates that there are two distinct regions to consider, which have changed after ligand binding. First region includes residues 64-76 that shows high fluctuations and it is comparable in both the ligand bound states. Second region (residues 99-112) indicates high fluctuations specifically associated with alkanolamine form binding and not seen for iminium form. Our data suggests that this second region distinguishes alkanolamine form induced structural changes from that of iminium form.

We found more structural changes in Lyz structure due to alkanolamine binding than the iminium binding from both MD and circular dichroism studies. Accordingly these binding differences might result in varied activity profile of two forms as reported from our experimental findings.

Next, we performed H-bond analysis to find the number of H-bonds between ligand and Lyz protein. Along the trajectory (10-100ns) average number of H-bonds for Lyz-iminium form complex was found to be 0.50 while 3.19 for Lyz-alkanolamine form complex per time frame. These values indicate more H-bonds and hence more binding between Lyz and alkanolamine form over Lyz and iminium form.

During 100ns simulation run both the chelerythrine forms remain associated with Lyz protein and have not come out of the binding pocket. Therefore, we analyzed all such interactions responsible for the binding. We found following pairs play important role in placing ligand in the binding pocket along the entire length of simulation (Table 4).

Both the chelerythrine forms have H-bond interaction with Trp-63 which plays a vital role in holding the ligand at its binding site. Alkanolamine form showed presence of more interactions where maximum stabilization was achieved from all the available functionally interacting groups. On one side both di-methoxy groups made H-bonds with Trp-63 while on another side dioxolo ring oxygen formed H-bond with Gln-57 and Asn-44. Middle -OH group which was initially forming H-bond with Glu-35, during simulation it orients towards Asp-52 and forms H-bond with it continuously, assisted partially by Asn-59 and Asn-46 H-bonds.

Iminium form has less than one H-bond per time-frame, out of which Trp-63 (-NH) formed H-bond with both the -OCH₃ groups. The interaction with inner -OCH₃ group was more prominent in both the forms. Overall, along the trajectory we witnessed iminium form binding was largely driven by hydrophobic interactions while alkanolamine form binding was largely from hydrogen bonding. This observation is in agreement with our calorimetric results.

Then we checked H-bond occurrence between ligand and water, which revealed average of 0.817 and 0.362 number of H-bonds per timeframe for alkanolamine form and iminium form

complexes, respectively. We also checked total number of H-bonds of water with both the Lyz-ligand complexes and found average value of 254.248 and 249.630 per time frame for lyz- alkanolamine form and lyz-iminium form complexes, respectively. Results indicate overall higher interactions with water for alkanolamine form complex than that for iminium form complex. MD analysis result goes hand in hand with our experimental findings to further support the higher affinity of alkanolamine than that of iminium form.

Comparing aggregation prone region with chelerythrine binding region

Human lysozyme is known to form amyloid fibrils in patients suffering from hereditary amyloidosis.⁷²⁻⁷⁴ For studying amyloid fibril formation Hen egg white lysozyme (HEWL) is already a proven model.⁷⁵ Studies on small molecules which involve targeting of amyloidogenic protein like Lyz are prevalent.⁷⁴ Considering this fact we have compared the chelerythrine binding region to that of the amyloidogenic aggregation prone region. Out of the several known regions chelerythrine binding occurs at some of the key aggregation prone residues. Previously 16 amino acids have been reported essential for aggregation activity,^{75,76} amongst them 9 amino acids are known to be very important and carry the ability of self-fibrillation called as K-peptide.^{75,77-78}

Binding pocket of chelerythrine consists of the following important residues: Glu-35, Asn-44, Asn-46, Asp-52, Gln-57, Trp-62, Trp-63, Ala-107, Trp-108, Val-109 and Arg-114. Most of them are known to have either direct or indirect contribution in fibril formation, coming from K-peptide (54-62)¹⁵ or amyloid state protelytically resistant (32-108)⁷⁹ regions, respectively. Trp-62 is thought to be the vital residue governing fibril formation.^{75, 80-82}

Chelerythrine binding pocket and K-peptide region nests well sandwiched between one another (Fig. 13). Contribution from both the regions is indispensable in the formation of chelerythrine binding pocket. Structurally, these two separate regions are inseparable and form the overall chelerythrine binding pocket.

The binding of iminium takes place at this key aggregation residue via Pi-sigma hydrophobic contact. Accordingly, iminium binding is expected to affect the aggregation event more intensely than alkanolamine binding.

Comparison of chelerythrine binding with sanguinarine

Chemically chelerythrine and sanguinarine share the common skeleton. Hence their molecular binding comparison has strong relevance to be addressed here in particular reference to our earlier report on sanguinarine.¹⁵ Both compounds effected quenching of the protein fluorescence that was found to be due to the formation of specific complexes at the ground state. The K_{sv} vales were however higher for chelerythrine over sanguinarine. Both chelerythrine analogs were bound closer to the site compared to the sanguinarine based on FRET distances. The binding affinity values from calorimetry experiment also revealed that chelerythrine analogues were bound more strongly than sanguinarine. Molecular docking experiment revealed preferably more binding of chelerythrine compared to sanguinarine, which was in accordance with our activity data. Comparative molecular recognition clearly demonstrated: 1) The location of putative binding site for benzophenanthridine alkaloids, was situated near the catalytic region 2) Binding event is pH dependent, where alkanolamine form always has higher binding than the iminium form. 3) The fate of higher binding depends on direct interactions at catalytic diode residues Glu-35 and Asp-52 of Lyz that affects the catalysis. 4) For good binding ligands with centrally located –OH group facing the binding pocket carry edge for binding over any other functional groups. The higher strength of binding of chelerythrine over sanguinarine was thus corroborated from modelling studies also.

Conclusions

Chelerythrine binds to lysozyme through ground state complex formation with affinity of the order of 10^5 M^{-1} . The binding affinity of the neutral alkanolamine form was stronger than that of the charged iminium form, which is similar to that observed for the binding of

sanguinarine. Fluorescence techniques predict that the interaction involves close contact with Trp-62 and 63 residues at the cleft region of the protein. Thermodynamics of the interaction revealed that the binding is endothermic for the iminium and exothermic for the alkanolamine. Hydrophobic interaction plays major role in the binding of the iminium and hydrogen bonding interaction in the case of the alkanolamine. Binding leads to strong secondary structural changes in the protein structure and this was confirmed from synchronous fluorescence and 3D fluorescence and circular dichroism data. Stronger conformational changes were induced in Lyz upon binding of the alkanolamine rather than the iminium. Binding mode analysis guided by docking studies confirmed that binding pocket resides at Glu-35, Asn-44, Asn-46, Asp-52, Gln-57, Trp-62, Trp-63, Ala-107, Trp-108, Val-109 and Arg-114 residues of Lyz protein. Amongst these residues rests two distinctly significant sites, one is orthosteric catalytic site and other is amyloidogenic aggregation prone region. Thus chelerythrine binding is expected to affect these two distinct and important activities. Simulations further provided dynamic view and evidences that are corroborating well with our spectroscopic and calorimetric observations. Mostly it answered how ligand binding, occupancy and associated structural changes happens over the time.

Binding at orthosteric site renders catalytic site unavailable for binding, leading to the inhibition of catalysis affecting normal Lyz function. Other important effect would be the inhibition of fibril formation, as caused by preoccupied chelerythrine, resulting in out of stock aggregation prone region. It projects the possible role of chelerythrine as a therapy for amyloid-related diseases. Collectively, the pharmacological actions of chelerythrine carry tremendous future, with the realization of mandatory further validation to establish chelerythrine as a novel drug.

Acknowledgements

This Council of Scientific and Industrial Research (CSIR) network project GenCODE (BSC0123) supported this work. C. Jash is a Senior Research Fellow of Department of Science and Technology, Govt. of India through the DST-INSPIRE scheme. P. Basu is a NET Senior Research Fellow of the University Grants Commission (UGC), Government of India. P.V. Payghan is a Senior Research Fellow under CSIR-Emeritus Scientist Scheme of Dr. Nanda Ghoshal. The authors appreciate the critical comments and suggestions of the anonymous reviewers that helped in improving the manuscript.

Electronic supplementary information

† Electronic supplementary information (ESI) available: Fig. S1–S8 and Table S1 See DOI:

References

1. G. M. Cragg and D. J. Newman, *Biochim. Biophys. Acta*, 2013, **1830**, 3670.
2. M. Maiti and G. Suresh Kumar, *J. Nucleic Acids*, 2010, **2010** Article ID 593408.
3. J. M. Herbert, J. M. Augereau, J. Gleyee and J. P. Maffrand, *Biochem. Biophys. Res. Commun.*, 1990, **172**, 993.
4. R. R. Weichselbaum, D. W. Kufe, S. J. Chmura and M. E. Dolan, Patent No. US 6426351.
5. J. O' Neill, M. Manion, P. Schwartz and D. M. Hockenbery, *Biochim. Biophys. Acta*, 2004, **1705**, 43.
6. Z. F. Zhang, Y. Guo, J. B. Zhang and X. H. Wei, *Arch. Pharm. Res.*, 2011, **34**, 791.
7. S. J. Chmura, M. E. Dolan, A. Cha, H. J. Mauceri, D. W. Kufe and R. R. Weichselbaum, *Clin. Cancer Res.*, 2000, **6**, 737.
8. S. Yamamoto, K. Seta, C. Morisco, S. F. Vatner and J. Sadoshima, *J. Mol. Cell. Cardiol.*, 2001, **33**, 1829.

9. M. Maiti and G. Suresh Kumar, *Med. Res. Rev.*, 2007, **27**, 649.
10. X. Cui, S. Lin and G. Yuan, *Int. J. Biol. Macromol.*, 2012, **50**, 996.
11. P. Basu and G. Suresh Kumar, *J. Photochem. Photobiol. B*, 2014, **138**, 282.
12. L. P. Bai, M. Hagihara, K. Nakatani and Z. H. Jiang, *Sci. Rep.*, 2014, **4**, 6767.
13. A. Das, R. Nandi and M. Maiti, *Photochem. Photobiol.*, 1992, **56**, 311.
14. M. Hossain, A. Y. Khan and G. Suresh Kumar, *J. Chem. Thermodyn.*, 2012, **47**, 90.
15. C. Jash, P. V. Payghan, N. Ghoshal and G. Suresh Kumar, *J. Phys. Chem. B*, 2014, **46**, 13077.
16. M. M. Chaturvedi, A. Kumar, B. G. Darnay, G. B. N. Chainy, S. Agarwal and B. B. Aggarwal, *J. Biol. Chem.*, 1997, **272**, 30129.
17. Y. H. Zhang, A. Bhunia, K. F. Wan, M. C. Lee, S. L. Chan, V. C. Yu and Y. K. Mok, *J. Mol. Biol.*, 2006, **364**, 536.
18. G. Pi, P. Ren, J. Yu, R. Shi, Z. Yuan and C. Wang, *J. Chromatogr. A*, 2008, **1192**, 17.
19. B. Masschalck and C. W. Michiels, *Crit. Rev. Microbiol.*, 2003, **29**, 191.
20. Ç. Mecitoglu, A. Yemenicioglu A. Arslanoglu, Z. S. Elmaci, F. Korel and A. E. Çetin, *Food. Res. Int.*, 2006, **39**, 12.
21. M. Buck, H. Schwalbe and C. M. Dobson, *Biochemistry*, 1995, **34**, 13219.
22. A. Ghosh, K. V. Brinda and S. Vishveahwara, *Biophys. J.*, 2007, **92**, 2523.
23. Z. R. Zhang, Q. Zheng, J. Han, G. P. Gao, J. Liu and T. Gong, *Biomaterials*, 2009, **30**, 1372.
24. Z. Gu, X. Zhu, S. Ni, Z. Su and H. M. Zhou, *Int. J. Biochem. Cell Biol.*, 2004, **36**, 795.
25. A. Das, R. Thakur, A. Dagar and A. Chakraborty, *Phys. Chem. Chem. Phys.*, 2014, **16**, 5368.
26. H. M. Zhang, B. P. Tang and Y. Q. Wang, *Mol. Biol. Rep.*, 2010, **37**, 3127.

27. C. Jash and G. Suresh Kumar, *RSC Adv.*, 2014, **4**, 12514.
28. J. Du and Z. Xia, *Anal. Lett.*, 2012, **45**, 2236.
29. M. N. N. Vieira, J. D. Figueroa-Villar, M. N. L. Meirelles, S. T. Ferreira and F. G. De Felice, *Cell Biochem. Biophys.*, 2006, **44**, 549.
30. R. Swaminathan, V. K. Ravi, S. Kumar, M. V. Kumar and N. Chandra, *Adv. Protein Chem. Struct. Biol.*, 2011, **84**, 63.
31. R. H. C. Strang, *Biochem. Educ.*, 1984, **12**, 57.
32. Y. Desfougères, A. Saint-Jalmes, A. Salonen, V. Vié, S. Beaufils, S. Pezenec, B. Desbat, V. Lechevalier and F. Nau, *Langmuir*, 2011, **27**, 14947.
33. J. R. Lakowicz, *Principles of fluorescence spectroscopy*, 3rd ed. Springer Science+Business Media. *New York*. 2006.
34. Schrödinger Maestro-v96012 9.6; Induced Fit Docking Protocol; Schrödinger LLC: New York, NY, 2013.
35. R. Diamond, *Mol. Biol.*, 1974, **82**, 371.
36. J. Dundas, Z. Ouyang, J. Tseng, A. Binkowski, Y. Turpaz and J. Liang, *Nucleic Acids Res.*, 2006, **34**, W116.
37. Z. Zhang, Y. Li, B. Lin, M. Schroeder and B. Huang, *Bioinformatics*, 2011, **27**, 2083.
38. H. Bingding, *Omics*, 2009, **13**, 325.
39. PyMOL Molecular Graphics System, version 1.3; DeLano Scientific: Palo Alto, CA, 2002.
40. Accelrys Software Inc., *Discovery Studio Modeling Environment*, Release 4.0, San Diego: Accelrys Software Inc., 2013.
41. N. Guex and M. C. Peitsch, *Electrophoresis*, 1997, **18**, 2714.
42. B. Hess, C. Kutzner, D. van der Spoel and E. Lindahl, *J. Chem. Theory Comput.*, 2008, **4**, 435.

43. C. Oostenbrink, A. Villa, A. E. Mark and W. F. Gunsteren, *J. Comput. Chem.*, 2004, **25**, 1656.
44. S. Canzar, M. El-Kebir, R. Pool, K. Elbassioni, A. K. Malde, A. E. Mark, D. P. Geerke, L. Stougie and G. W. Klau, *J. Comp. Biol.*, 2013, **20**, 188.
45. K. B. Koziara, M. Stroet, A. K. Malde and A. E. Mark, *J. Comput. Aided Mol. Des.*, 2014, **28**, 221.
46. H. Berendsen, J. Postma, W. Gunsteren and J. Hermans, Interaction Models for Water in Relation to Protein Hydration. In: Intermolecular Forces; Pullman, B., Ed.; D. Reidel Publishing Co., *Amsterdam*, 1981, 331.
47. G. Bussi, D. Donadio and M. Parrinello, *J. Chem. Phys.*, 2007, **126**, 014101.
48. M. Parrinello and A. Rahman, *J. Appl. Phys.*, 1981, **52**, 7182.
49. T. Darden, D. York and L. Pedersen, *J. Chem. Phys.*, 1993, **98**, 10089.
50. B. Hess, H. Bekker, H. J. C. Berendsen and J. Fraaije, *J. Comput. Chem.*, 1997, **18**, 1463.
51. S. Páll and B. Hess, *Comput. Phys. Commun.*, 2013, **184**, 2641.
52. P. Basu, D. Bhowmik and G. Suresh Kumar, *J. Photochem. Photobiol. B*, 2013, **129**, 57.
53. H. A. Benesi and J. H. Hildebrand, *J. Am. Chem. Soc.*, 1949, **71**, 2703.
54. P. Qin, B. Su and R. Liu, *Mol. BioSyst.*, 2012, **8**, 1222.
55. S. Tabassum, W. M. Al-Asbahy, M. Afzal, F. Arjmand and R. H. Khan, *Mol. BioSyst.*, 2012, **8**, 2424.
56. A. P. Demchenko. *Springer-Verlag, Berlin*. 1986, **DM 198**, 312.
57. Z. Chi and S. A. Asher, *J. Phys. Chem. B*, 1998, **102**, 9595.
58. B. C. MacDonald, S. J. Lvin and H. Patterson, *Anal. Chim. Acta*, 1997, **338**, 155.
59. S. Hazra and G. Suresh Kumar, *J. Phys. Chem. B*, 2014, **118**, 3771.

60. J. R. Lakowicz, *Principles of Fluorescence Spectroscopy*; Plenum Press: New York, 1999.
61. W. Peng, F. Ding, Y. K. Peng, Y. T. Jiang and L. Zhang, *J. Agric. Food Chem.*, 2013, **61**, 12415.
62. K. Shanmugaraj, S. Anandakumar and M. Ilanchelian, *Dyes Pigm.*, 2015, **112**, 210.
63. B. Cardenas, G. Sanchez-Obrero, R. Madueno, J. M. Sevilla, M. Blazquez and T. Pineda, *J. Phys. Chem. C*, 2014, **118**, 22274.
64. L. Stryer, *J. Mol. Biol.*, 1965, **13**, 482.
65. L. Stryer, *J. Biol. Chem.*, 2012, **287**, 15164.
66. J. B. F. Lloyd, *Nat. Phys. Sci.*, 1971, **231**, 64.
67. J. N. Miller, *Proc. Anal. Div. Chem. Soc.*, 1979, **16**, 203.
68. M. A. Landau, M. N. Markovich and L. A. Piruzyan *Biochim. Biophys. Acta*, 1977, **493**, 1.
69. R. S. Spolar and M. T. Record Jr., *Science*, 1994, **263**, 777.
70. H. D. Bian, H. R. Zhang, Q. Yu, Z. F. Chen and H. Liang, *Chem. Pharm. Bull.*, 2007, **55**, 871.
71. G. R. Desiraju, *Acc. Chem. Res.*, 1996, **29**, 441.
72. M. B. Pepys, P. N. Hawkins, D. R. Booth, D. M. Vigushin, G. A. Tennent, A. K. Soutar, N. Totty, O. Nguyen, C. C Blake and C. J. Terry et. al., *Nature*, 1993, **362**, 553.
73. S. Valleix, S. Drunat, J. B. Philit, D. Adoue, J. C. Piette and D. Droz, et al., *Kidney Int.*, 2002, **61**, 907.
74. M., Yazaki, S. A. Farrell and M. D. Benson, *Kidney Int.*, 2003, **63**, 1652.
75. Y. Tokunaga, Y. Sakakibara, Y. Kamada, K. Watanabe and Y. Sugimoto, *Int. J. Biol. Sci.*, 2013, **9**, 219.

76. J. He, Y. Wang, A. K. Chang, L. Xu, N. Wang, X. Chong, H. Li, B. Zhang, G. W. Jones and Y. Song, *J. Agric. Food Chem.*, 2014, **62**, 9442.
77. Y. Sugimoto, Y. Kamada, Y. Tokunaga, H. Shinohara, M. Matsumoto, T. Kusakabe, T. Ohkuri and T. Ueda, *Biochem. Cell Biol.*, 2011, **89**, 533.
78. T. A. Pertinhez, M. Bouchard, R. A. Smith, C. M. Dobson and L. J. Smith, *FEBS Lett.*, 2002, **529**, 193.
79. G. G. Tartaglia, A. P. Pawar, S. Campioni, C. M. Dobson, F. Chiti and M. Vendruscolo, *J. Mol. Biol.*, 2008, **380**, 425.
80. T. Ohkuri, S. Shioi, T. Imoto and T. Ueda, *J. Mol. Biol.*, 2009, **347**, 159.
81. R. Zhou, M. Eleftheriou, A. K. Royyuru and B. J. Berne, *Proc. Natl. Acad. Sci. USA*, 2007, **104**, 5824.
82. T. Mishima, T. Ohkuri, A. Monji, T. Imoto and T. Ueda, *Biochem. Biophys. Res. Commun.*, 2007, **356**, 769.

Figure legends

Fig. 1 Chemical structures of two forms of chelerythrine. The lower panel shows the corresponding absorption spectra of the iminium and alkanolamine form in 10 mM citrate-phosphate (pH 6.4) and 10 mM carbonate-bicarbonate (pH 9.2) buffer, respectively.

Fig. 2 Representative absorption spectra of Lyz (1.07 μM) treated with (A) 0, 1, 2, 3, 4, 5 and 7 μM (curves 1–7) of iminium and (B) 0, 1, 2, 3, 4, 5 and 7 μM (curves 1–7) of alkanolamine form of chelerythrine. Inset represents the corresponding Benesi-Hildebrand plots.

Fig. 3 Lyz (1 μM) treated with various concentrations of (A) iminium and (B) alkanolamine form in 10 mM citrate-Phosphate buffer, pH = 6.4 and 10 mM carbonate-bicarbonate buffer, pH = 9.2, respectively. In panel (A) curves (1–12) denote 0, 0.5, 1, 2, 3, 4, 5, 6, 7, 8, 9 and 12 μM of iminium and (B) curves (1–12) denote 0, 0.5, 1, 2, 3, 4, 5, 6, 7, 8, 9 and 11 μM of alkanolamine form of chelerythrine, respectively.

Fig. 4 (A) Steady state fluorescence spectra of 1 μM chelerythrine iminium and alkanolamine form. (B) Relative fluorescence intensity plot for the iminium (closed square) and alkanolamine (closed circle) form treated with different concentration of Lyz.

Fig. 5 ANS displacement assay for the Lyz treated with different concentration of (A) iminium and (B) alkanolamine form of chelerythrine at different Lyz:ANS ratio.

Fig. 6 Intrinsic circular dichroism (far UV CD) spectra of Lyz (5 μM) treated with various concentrations of (A) iminium and (B) alkanolamine form of chelerythrine. In panel (A) curves (1–6) denote 0, 5, 10, 15, 20 and 30 μM of iminium and (B) curves (1–6) denote 0, 5, 10, 15, 20 and 30 μM of alkanolamine form of chelerythrine, respectively.

Fig. 7 ITC profiles for the binding of chelerythrine to Lyz. Top panels present raw results for the sequential injection of Lyz of 0.5 mM and 0.8 mM into solutions of (A) iminium (50 μM), and (B) alkanolamine (50 μM) at 298 K, and dilution of Lyz into respective buffer (not in

scale). The bottom panels show the integrated heat results after correction of heat of dilution against the mole ratio of Lyz/chelerythrine. The data points were fitted to one site model and the solid lines represent the best-fit data.

Fig. 8 Crucial H-bond interactions both classical and non-classical for A) iminium and B) alkanolmine (R). Black dotted line for classical H-bonds and blue for non-classical.

Fig. 9 Surface representation showing hydrophobicity and electrostatic interactions for A) iminium and B) alkanolmine (R). Hydrophobic scale -3 to 3, showing hydrophilic (blue) to hydrophobic (gray). Pink dotted line for Pi-hydrophobic contacts for: alkanolamine Val-109 and iminium Ala-107, Val-109. Purple for Pi-sigma at Trp-62 in iminium form. Orange dotted line represents electrostatic interactions.

Fig. 10 Backbone RMSD Plot for apo, Lyz-imuminium and Lyz-alkanolamine bound states.

Fig. 11 Radius of gyration plot for apo, Lyz-imuminium and Lyz-alkanolamine forms. (analysis form 10-100ns MD simulation run).

Fig. 12 Residue-wise root mean square fluctuations for apo, Lyz-imuminium and Lyz-alkanolamine forms. (analysis form 10-100ns MD simulation run).

Fig. 13 Surface representation of chelerythrine binding pocket and aggregation Prone K-peptide region: Showing bound iminium form, purple for K-peptide residues (dark purple for crucial Trp-62), blue solely for binding pocket residues.

Table 1. Binding Data Derived for Chelerythrine Binding to Lyz from Spectrofluorimetric Studies at Different Temperatures^a

chelerythrine	temp.	$10^{-5} (K_{SV})$	$10^{-13} (k_q)$	$10^{-5} (K_A)$	n	10^{-5}
	(K)	$/M^{-1}$	$/M^{-1} s^{-1}$	$/M^{-1}$		$(K_{LB})/M^{-1}$
	288	1.72±0.16	8.27	1.67±0.11	1.01±0.02	1.65±0.19
iminium	298	1.23±0.03	5.91	1.21±0.11	1.03±0.03	1.21±0.08
	308	0.98±0.09	4.71	0.95±0.06	1.05±0.04	0.95±0.07
	288	10.5±1.92	53.8	10.2±1.2	1.01±0.01	10.2±1.56
alkanolamine	298	7.42±0.84	38.1	7.26±0.78	1.01±0.02	7.18±0.80
	308	4.08±0.66	20.9	3.96±0.55	1.00±0.03	3.81±0.52

^a($\tau_0 = 2.08$ ns at pH 6.4 and 1.95 ns at pH 9.2). The data presented are averages of four determinations.

K_{SV} is the Stern–Volmer quenching constant, K_A is the binding constant, and K_{LB} is the static quenching constant from Lineweaver–Burk equation. The errors are based on standard deviations.

Table 2. Thermodynamic Parameters for the Binding of Chelerythrine with Lyz from ITC at Different Temperatures^a

		binding		(ΔH^0)	$(T\Delta S^0)$	(ΔG^0)	(ΔC_p^0)
chelerythrine	temp(K)	constant	N	kcal/ mole	kcal/ mole	kcal/ mole	(cal/mole. K)
		(K_b) (M ⁻¹)					
	288	$(1.84 \pm .27) \times 10^5$	0.80	0.64 ± 0.13	7.58	-6.93 ± 0.13	
iminium	298	$(1.29 \pm .08) \times 10^5$	0.87	0.62 ± 0.98	7.60	-6.98 ± 0.98	-5.72
	308	$(1.04 \pm .05) \times 10^5$	0.94	0.52 ± 1.06	7.61	-7.08 ± 1.06	
alkanolamine	288	$(1.44 \pm .33) \times 10^6$	1.17	-0.94 ± 0.09	7.17	-8.11 ± 0.09	
	298	$(7.79 \pm .08) \times 10^5$	0.87	-1.26 ± 0.06	6.77	-8.03 ± 0.06	-30.3
	308	$(4.06 \pm .18) \times 10^5$	1.29	-1.55 ± 0.09	6.35	-7.89 ± 0.09	

^a The data presented are averages of four determinations. All the data in this table are derived from ITC experiments conducted in either 10 mM [Na⁺] of CP buffer, pH 6.4 or CB buffer, pH 9.2 and are averages of four determinations. K_b and ΔH^0 values were determined from ITC profiles fitting to Origin 7.0 software as described in the text. The errors are based on standard deviations.

Table 3. Results from Molecular Docking Studies: For the Binding of Alkanolamine and Iminium at Lyz Protein

chelerythrine	glide Score	H-bonds classical	H-bonds Non- classical	electrostatic interactions	hydrophobic interactions
alkanolamine	-9.796	Glu-35	Asp-52	Asp-52	Asn-46
		Trp-63	Ala-107		Val-109
		Arg-114	Trp108		
iminium	-6.368	Trp-63	Gln-57	Glu-35	Trp-62
				Asp-52	Ala-107

Table 4. H-bond Interaction Analysis from MD Studies for 10-100ns Run

chelerythrine	H-bonding residue	partner from Ligand	avg. number of H-bonds per time-frame
	Trp-63 (-NH)	-OCH3 (outer)	0.388
	Trp-63 (-NH)	-OCH3 (inner)	0.661
alkanolamine	Asp-52 (COO ⁻)	-OH	1.000
	Asn-44 (-NH ₂)	-O- of dioxolo ring	0.198
	Gln-57 (-NH ₂)	-O- of dioxolo ring	0.653
iminium	Trp-63 (-NH)	-OCH3 (outer)	0.060
	Trp-63 (-NH)	-OCH3 (inner)	0.355

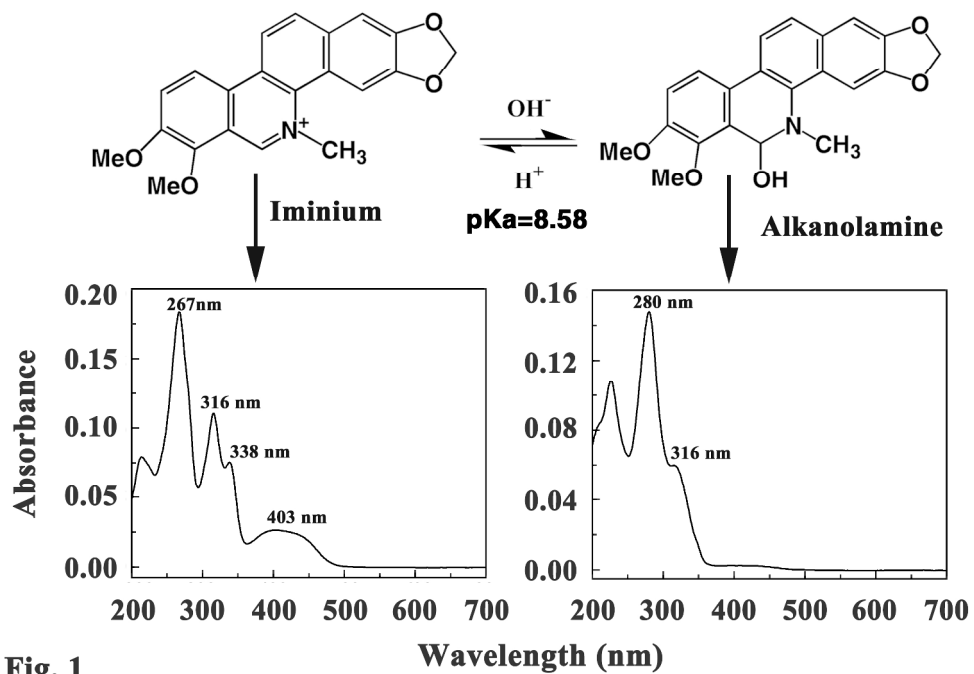
**Fig. 1**

Fig. 1 Chemical structures of two forms of chelerythrine. The lower panel shows the corresponding absorption spectra of the iminium and alkanolamine form in 10 mM citrate-phosphate (pH 6.4) and 10 mM carbonate-bicarbonate (pH 9.2) buffer, respectively.

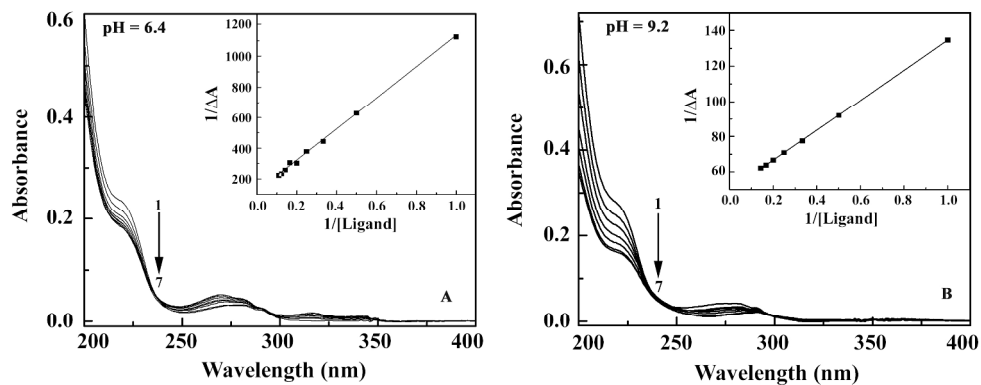
**Fig. 2**

Fig. 2 Representative absorption spectra of Lyz (1.07 μM) treated with (A) 0, 1, 2, 3, 4, 5 and 7 μM (curves 1–7) of iminium and (B) 0, 1, 2, 3, 4, 5 and 7 μM (curves 1–7) of alkanolamine form of chelerythrine. Inset represents the corresponding Benesi-Hildebrand plots.
472x197mm (150 x 150 DPI)

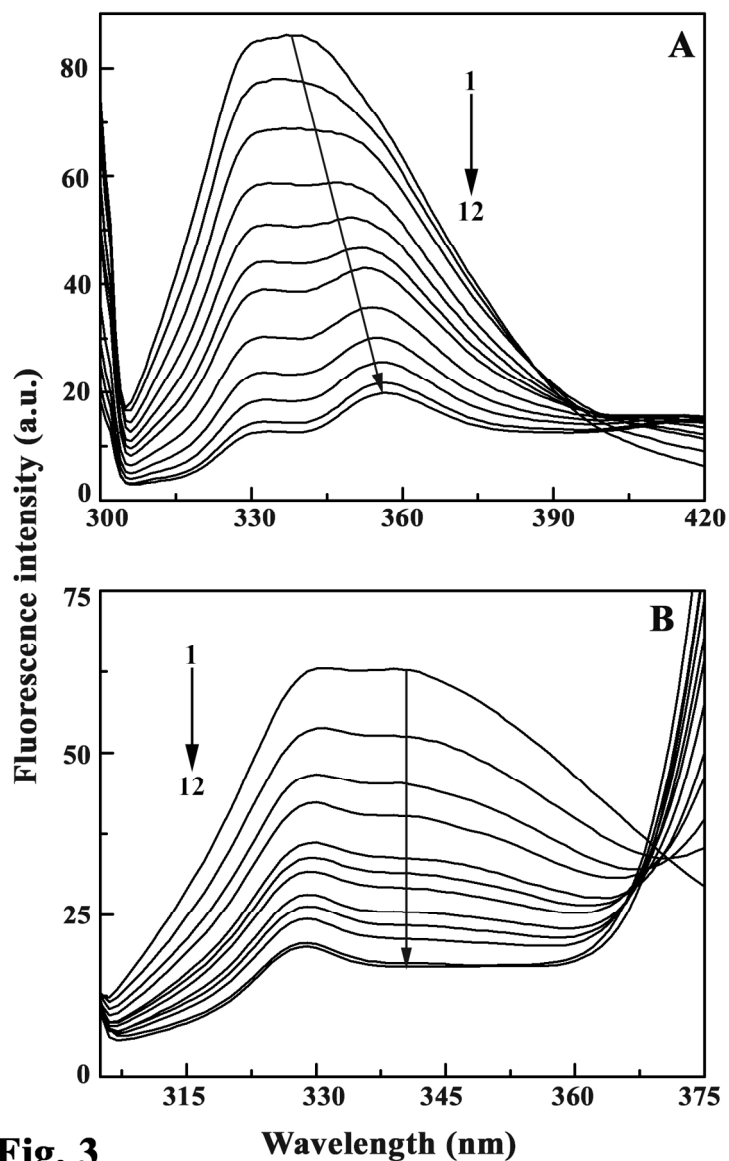
**Fig. 3**

Fig. 3 Lyz ($1\mu\text{M}$) treated with various concentrations of (A) iminium and (B) alkanolamine form in 10 mM citrate-Phosphate buffer, pH = 6.4 and 10 mM carbonate-bicarbonate buffer, pH= 9.2, respectively. In panel (A) curves (1-12) denote 0, 0.5, 1, 2, 3, 4, 5, 6, 7, 8, 9 and 12 μM of iminium and (B) curves (1-12) denote 0, 0.5, 1, 2, 3, 4, 5, 6, 7, 8, 9 and 11 μM of alkanolamine form of chelerythrine, respectively.
235x360mm (150 x 150 DPI)

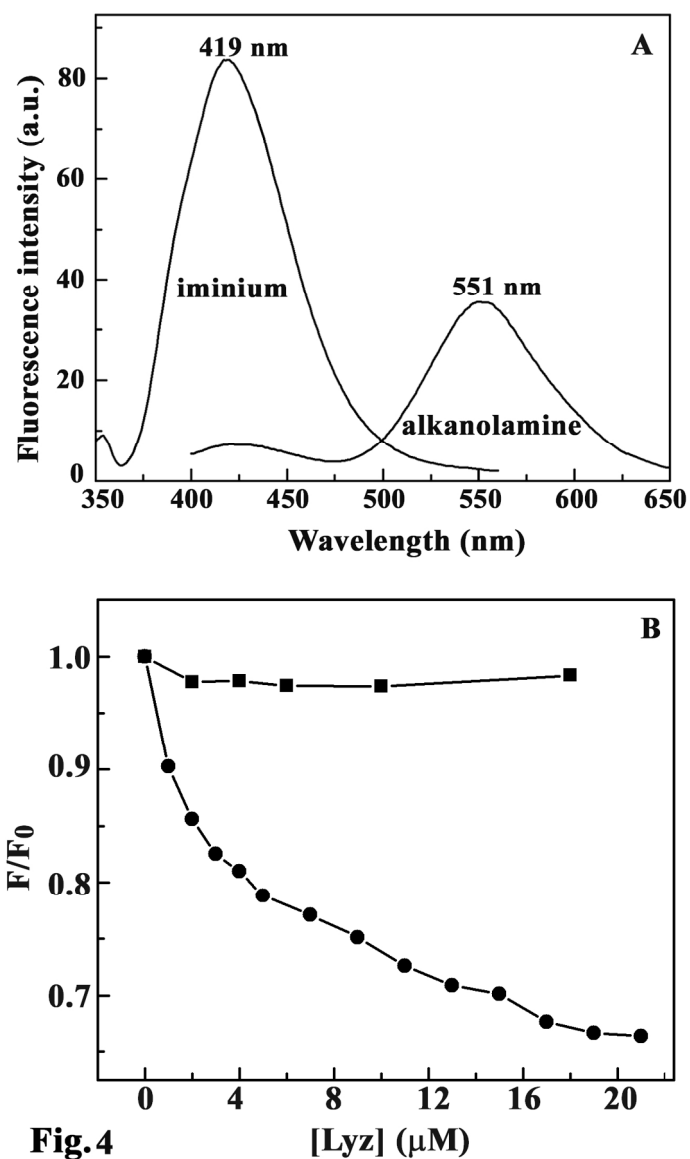


Fig. 4 (A) Steady state fluorescence spectra of 1 μM chelerythrine iminium and alkanolamine form. (B) Relative fluorescence intensity plot for the iminium (closed square) and alkanolamine (closed circle) form treated with different concentration of Lyz.
229x387mm (150 x 150 DPI)

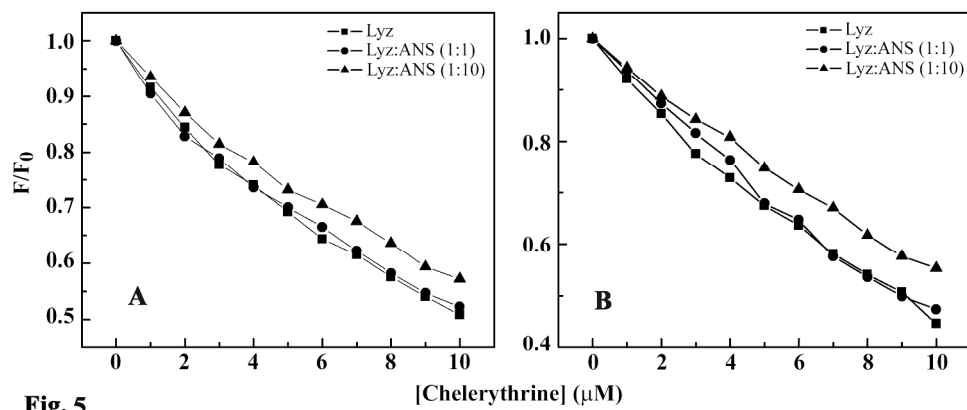


Fig. 5

Fig. 5 ANS displacement assay for the Lyz treated with different concentration of (A) iminium and (B) alkanolamine form of chelerythrine at different Lyz:ANS ratio.
462x199mm (150 x 150 DPI)

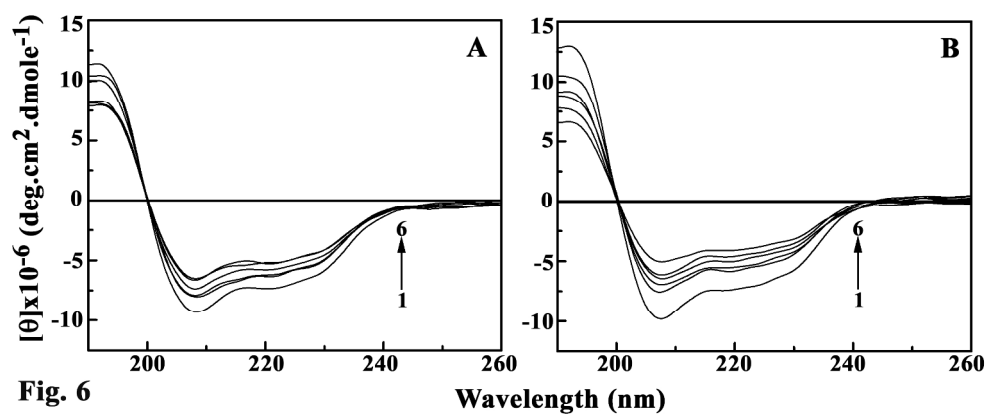


Fig. 6 Intrinsic circular dichroism (far UV CD) spectra of Lyz (5 μM) treated with various concentrations of (A) iminium and (B) alkanolamine form of chelerythrine. In panel (A) curves (1–6) denote 0, 5, 10, 15, 20 and 30 μM of iminium and (B) curves (1–6) denote 0, 5, 10, 15, 20 and 30 μM of alkanolamine form of chelerythrine, respectively.

246x103mm (300 x 300 DPI)

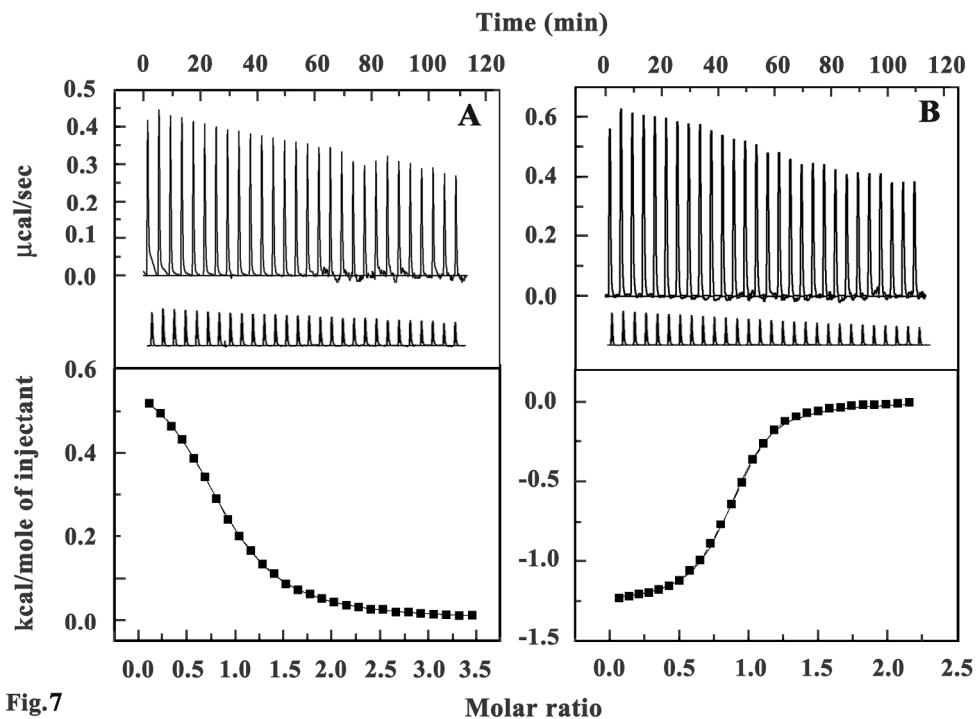


Fig.7

Fig. 7 ITC profiles for the binding of chelerythrine to Lyz. Top panels present raw results for the sequential injection of Lyz of 0.5 mM and 0.8 mM into solutions of (A) iminium (50 μM), and (B) alkanolamine (50 μM) at 298 K, and dilution of Lyz into respective buffer (not in scale). The bottom panels show the integrated heat results after correction of heat of dilution against the mole ratio of Lyz/chelerythrine. The data points were fitted to one site model and the solid lines represent the best-fit data.

377x277mm (150 x 150 DPI)

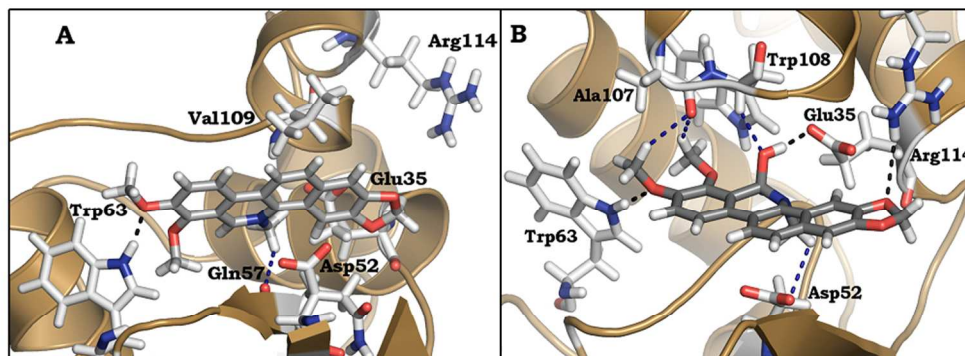
**Fig. 8**

Fig. 8 Crucial H-bond interactions both classical and non-classical for A) iminium and B) alkanolmine (R). Black dotted line for classical H-bonds and blue for non-classical.
273x115mm (96 x 96 DPI)

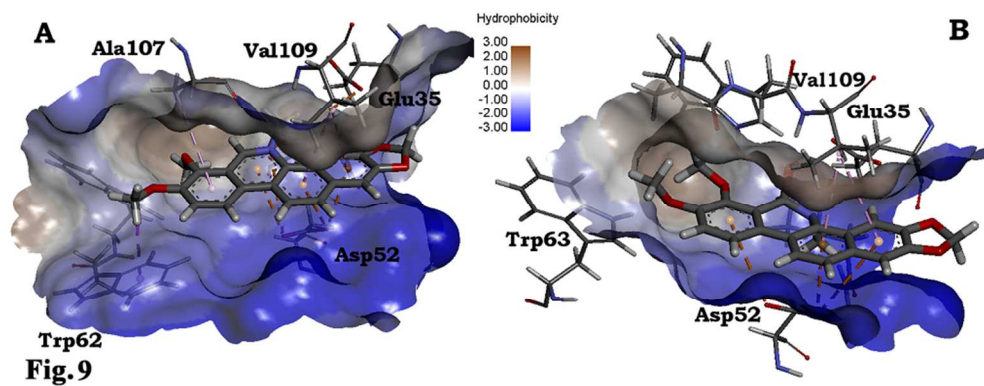


Fig. 9 Surface representation showing hydrophobicity and electrostatic interactions for A) iminium and B) alkanolmine (R). Hydrophobic scale -3 to 3, showing hydrophilic (blue) to hydrophobic (gray). Pink dotted line for Pi-hydrophobic contacts for: alkanolamine Val-109 and iminium Ala-107, Val-109. Purple for Pi-sigma at Trp-62 in iminium form. Orange dotted line represents electrostatic interactions.

272x104mm (96 x 96 DPI)

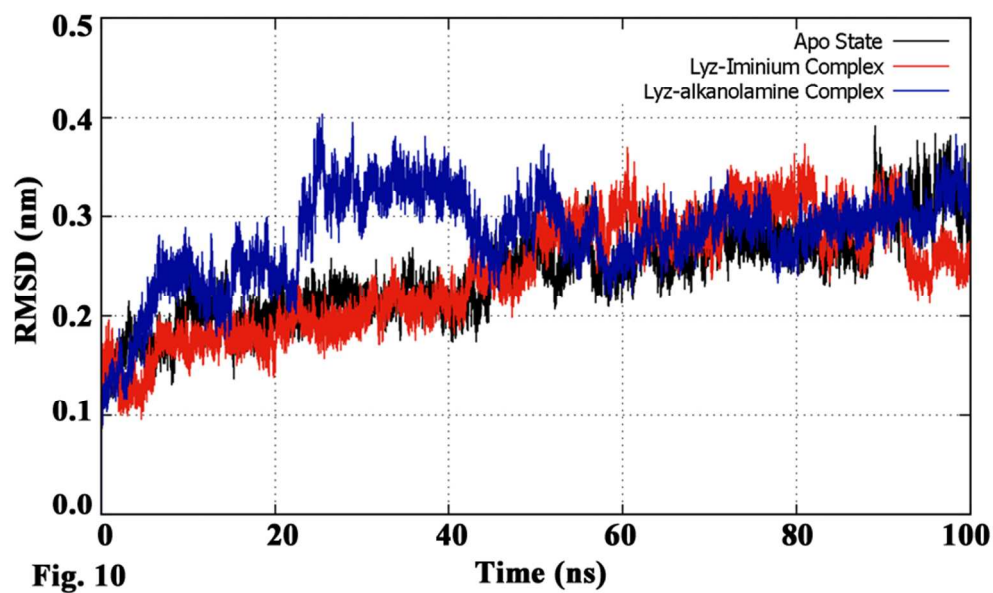


Fig. 10 Backbone RMSD Plot for apo, Lyz-iminium and Lyz-alkanolamine bound states.
344x215mm (72 x 72 DPI)

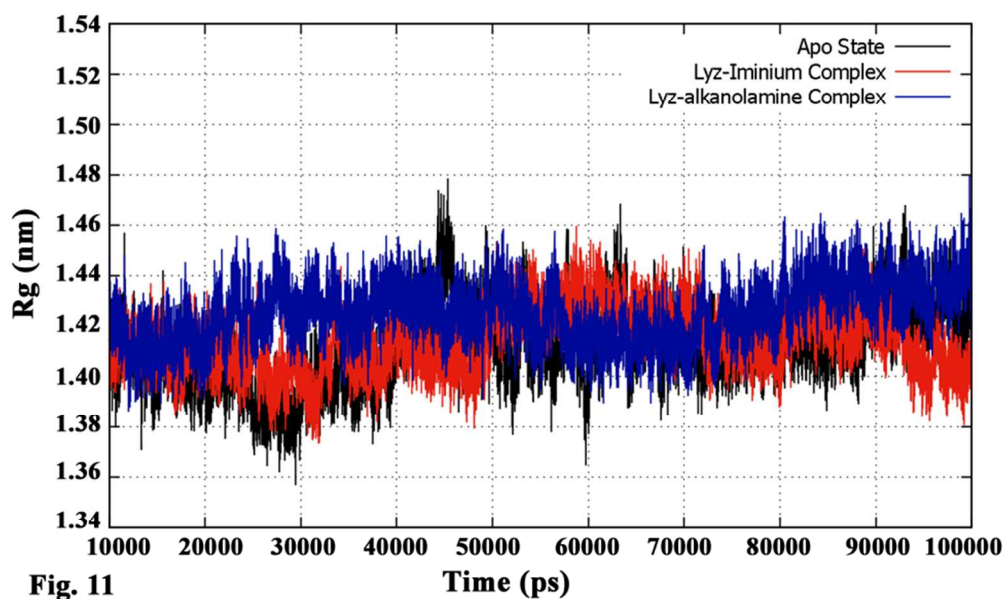


Fig. 11

Fig. 11 Radius of gyration plot for apo, Lyz-iminium and Lyz-alkanolamine forms. (analysis from 10-100ns MD simulation run).
343x215mm (72 x 72 DPI)

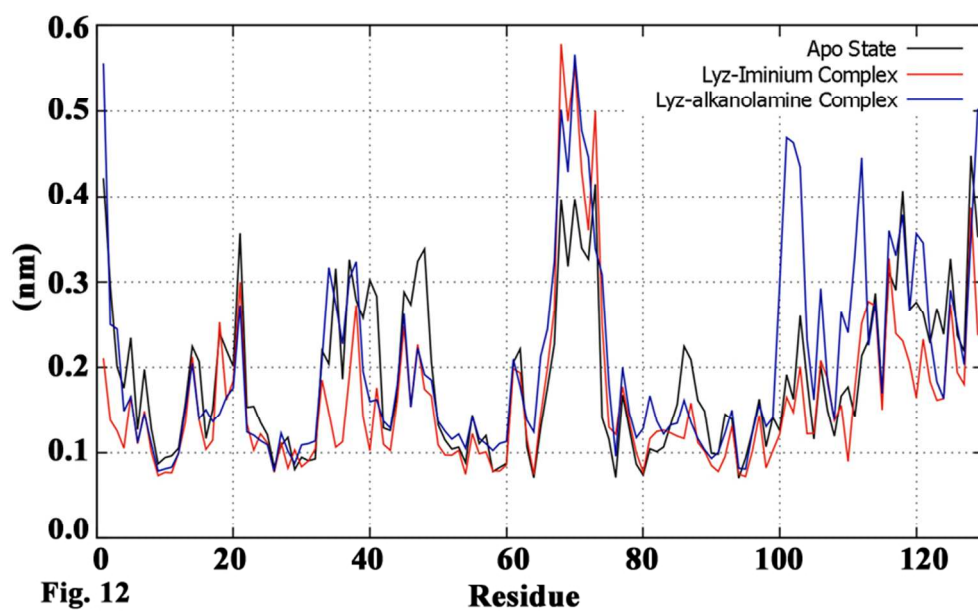


Fig. 12 Residue-wise root mean square fluctuations for apo, Lyz-iminium and Lyz-alkanolamine forms. (analysis from 10-100ns MD simulation run).
337x215mm (72 x 72 DPI)

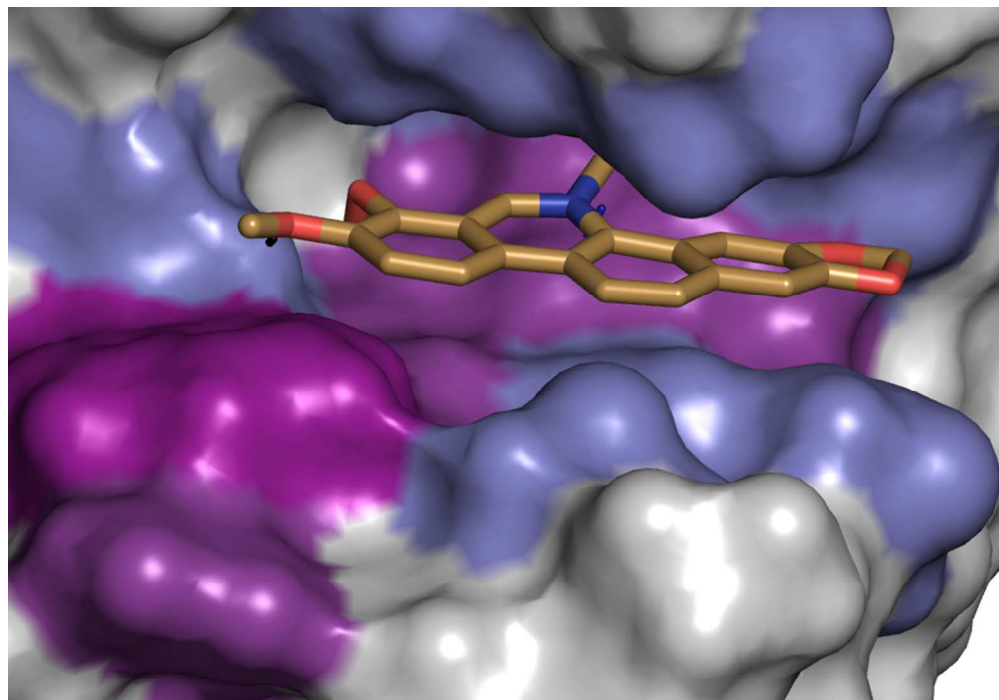


Fig. 13

Fig. 13 Surface representation of chelerythrine binding pocket and aggregation-prone K-peptide region: Showing bound iminium form, purple for K-peptide residues (dark purple for crucial Trp-62), blue solely for binding pocket residues.
322x246mm (72 x 72 DPI)